

Multi-angle effects in self-induced oscillations for different supernova neutrino fluxes

Alessandro Mirizzi¹ and Ricard Tomàs¹

¹*II Institut für Theoretische Physik, Universität Hamburg,
Luruper Chaussee 149, 22761 Hamburg, Germany*

The non-isotropic nature of the neutrino emission from a supernova (SN) core might potentially affect the flavor evolution of the neutrino ensemble, via neutrino-neutrino interactions in the deepest SN regions. We investigate the dependence of these “multi-angle effects” on the original SN neutrino fluxes in a three-flavor framework. We show that the pattern of the spectral crossings (energies where $F_{\nu_e} = F_{\nu_x}$, and $F_{\bar{\nu}_e} = F_{\bar{\nu}_x}$) is crucial in determining the impact of multi-angle effects on the flavor evolution. For neutrino spectra presenting only a single-crossing, synchronization of different angular modes prevails over multi-angle effects, producing the known “quasi single-angle” evolution. Conversely, in the presence of spectra with multiple crossing energies, synchronization is not stable. In this situation, multi-angle effects would produce a sizable delay in the onset of the flavor conversions, as recently observed. We show that, due to the only partial adiabaticity of the evolution at large radii, the multi-angle suppression can be so strong to dramatically affect the final oscillated neutrino spectra. In particular three-flavor effects, associated with the solar parameters, could be washed-out in multi-angle simulations.

PACS numbers: 14.60.Pq, 97.60.Bw

I. INTRODUCTION

The characterization of the flavor conversions for neutrinos emitted by a stellar collapse is a field of intense activity. In particular, the flavor transformation probabilities in supernovae (SNe) not only depend on the matter background [1, 2], but also on the neutrino fluxes themselves: neutrino-neutrino interactions provide a nonlinear term in the equations of motion [3–5] that causes collective flavor transformations [6–16]. Only recently [17–19] it has been fully appreciated that in the SN context these collective effects give rise to qualitatively new phenomena (see, e.g., [20] for a recent review). The main consequence of this unusual type of flavor transitions is an exchange of the spectrum of the electron species ν_e ($\bar{\nu}_e$) with the non-electron ones ν_x ($\bar{\nu}_x$) in certain energy intervals. These flavor exchanges are called “swaps” marked by the “splits”, which are the boundary features at the edges of each swap interval [18, 20–31]. The location and the number of these splits, as well as their dependence on the neutrino mass hierarchy, is crucially dependent on the flux ordering among different neutrino species [32, 33].

In this context, one of the main complication in the simulation of the flavor evolution is that the flux of neutrinos emitted from a supernova core is far from isotropic. The current-current nature of the weak-interaction Hamiltonian implies that the interaction energy between neutrinos of momenta \mathbf{p} and \mathbf{q} is proportional to $(1 - \mathbf{v}_\mathbf{p} \cdot \mathbf{v}_\mathbf{q})$, where $\mathbf{v}_\mathbf{p}$ is the neutrino velocity [6, 34]. In a non-isotropic medium this velocity-dependent term would not average to zero, producing a different refractive index for neutrinos propagating on different trajectories. This is the origin of the so-called “multi-angle effects” [18], which hinder the maintenance of the coherent oscillation behavior for different neutrino modes [21, 35–37]. In [35] it has been shown that in

a dense neutrino gas initially composed of only ν_e and $\bar{\nu}_e$ with equal fluxes, multi-angles effects would rapidly lead to flavor decoherence, resulting in flux equilibration among electron and non-electron (anti)neutrino species. On the other hand, in the presence of relevant flavor asymmetries between ν_e and $\bar{\nu}_e$ multi-angle effects can be suppressed. In particular, during the early SN accretion phase, one expects as neutrino flux ordering $\Phi_{\nu_e} \gg \Phi_{\bar{\nu}_e} \gg \Phi_{\nu_x} = \Phi_{\bar{\nu}_x}$ [38–40], defined in terms of the total neutrino number fluxes Φ_ν for the different flavors. This case would practically correspond to neutrino spectra with a *single crossing* point at $E \rightarrow \infty$ (where $F_{\nu_e} = F_{\nu_x}$, and $F_{\bar{\nu}_e} = F_{\bar{\nu}_x}$) since $F_{\nu_e}(E) > F_{\nu_x}(E)$ for all the relevant energies (and analogously for $\bar{\nu}$). For spectra with a single crossing, it has been shown in [36] that the presence of significant flavor asymmetries between ν_e and $\bar{\nu}_e$ fluxes guarantees the synchronization of different angular modes at low-radii ($r \lesssim 100$ km), so that essentially nothing happens close to the neutrinosphere because the in-medium mixing is extremely small. Therefore, the possible onset of multi-angle effects is delayed after the synchronization phase. Then, the flavor evolution is adiabatic to produce spectral splits and swaps but not enough to allow the multi-angle instability to grow and produce significant decoherence effects. Therefore, the resultant neutrino flavor conversions would be described by an effective “quasi single-angle” behavior. In this case, the self-induced spectral swaps and splits would be only marginal smeared by multi-angle effects, as explicitly shown in [18, 21, 22]. This reassuring result has been taken as granted in most of the further studies that typically adopted the averaged single-angle approximation.

However, this nice picture does not represent the

end of the story for multi-angle effects.¹ A different result has been recently shown in [42], where multi-angle effects are explored, assuming a flux ordering of the type $\Phi_{\nu_x} \gtrsim \Phi_{\nu_e} \gtrsim \Phi_{\bar{\nu}_e}$, possible during the SN cooling phase, where one expects a moderate flavor hierarchy among different species and a “cross-over” among non-electron and electron species is possible [38–40]. This case would correspond to neutrino spectra with *multiple crossing* points, i.e. with $F_{\nu_e}(E) > F_{\nu_x}(E)$ at lower energies, and $F_{\nu_e}(E) < F_{\nu_x}(E)$ at higher energies (and analogously for $\bar{\nu}$). For such spectra, it has been shown in [43] that the synchronization is not a stable solution for a neutrino gas in presence of a large neutrino density. Therefore, collective flavor conversions would be possible at low-radii in the single-angle scheme [43], in a region where one would have naively expected synchronization. However, it has been shown in [42] that the presence of a large dispersion in the neutrino-neutrino refractive index, induced by multi-angle effects, seems to block the development of these collective flavor conversions close to the neutrinosphere. This recent result extends the finding obtained with a toy model in [43]. The delay of the self-induced flavor conversions for this case is also visible in the multi-angle simulations in [44]. So, it is apparent that multi-angle effects are relevant not only for fluxes with small flavor asymmetries, where they trigger a quick flavor *decoherence*, but also in cases of spectra with multiple crossing points, where multi-angle effects can *suppress* flavor conversions at low-radii.

Triggered by the contrasting impact of the multi-angle effects for fluxes typical of the accretion and cooling phase, we take a closer look at the dependence of these effects on the neutrino flux ordering. The plan of our work is as follows. In Sec. II we introduce our supernova flux models, and describe the equations for the flavor conversions in the multi-angle and single-angle case. In Sec. III we show and explain our numerical results for the single-angle and multi-angle flavor evolution for some representative choices of SN neutrino fluxes. In particular, we select three cases corresponding respectively to *a*) single-crossed neutrino spectrum with $\Phi_{\nu_e} \gg \Phi_{\bar{\nu}_e} \gg \Phi_{\nu_x}$, producing a “quasi single-angle” flavor evolution, *b*) multiple-crossed spectrum with $\Phi_{\nu_x} \gtrsim \Phi_{\nu_e} \gtrsim \Phi_{\bar{\nu}_e}$, where single-angle and multi-angle evolutions give significantly different final neutrino spectra, *c*) small flavor asymmetries, i.e. $\Phi_{\nu_e} \approx \Phi_{\bar{\nu}_e} \approx \Phi_{\nu_x}$, where the multi-angle suppression is small, and multi-angle decoherence produces a partial flavor equilibration among the different species. Finally, in Sec. IV we draw inferences from our results and summarize. Technical aspects are discussed in the Appendix.

II. SUPERNOVA NEUTRINO FLUXES AND EQUATIONS OF MOTION

A. Supernova flux models

In the presence of neutrino-neutrino interactions the flavor conversions for SN neutrinos are described by non-linear equations. Therefore, SN neutrino oscillations will crucially depend on the initial neutrino fluxes. We define F_{ν_α} as the number flux of a given neutrino species ν_α emitted with energy E in any direction at the neutrinosphere. In a supernova ν_e and $\bar{\nu}_e$ are distinguished from other flavors due to their charged-current interactions. The ν_μ , ν_τ and their antiparticles, on the other hand, are produced at practically identical rates. Following the standard terminology [45], we define the two relevant non-electron flavor states as $\nu_{x,y} = \cos \theta_{23} \nu_\mu \mp \cos \theta_{23} \nu_\tau$, where $\theta_{23} \approx \pi/4$ is the atmospheric mixing angle. Since the initial ν_x and ν_y fluxes are identical, the primary neutrino fluxes are best expressed in terms of ν_e , $\bar{\nu}_e$ and ν_x . For half-isotropic emission these three relevant SN ν original neutrino number fluxes for the different species are given by [21]

$$F_{\nu_\alpha}^0(E) = \Phi_{\nu_\alpha}^0 \varphi_{\nu_\alpha}(E), \quad (1)$$

where

$$\Phi_{\nu_\alpha}^0 = \frac{1}{4\pi^2 R^2} \frac{L_{\nu_\alpha}}{\langle E_{\nu_\alpha} \rangle} \quad (2)$$

is the total number flux at the neutrinosphere radius R , that in our numerical examples we will take $R = 10$ km. The neutrino luminosity is L_{ν_α} and the neutrino average energy $\langle E_{\nu_\alpha} \rangle$. The function $\varphi_{\nu_\alpha}(E)$ is the normalized neutrino spectrum ($\int dE \varphi_{\nu_\alpha} = 1$) and parametrized as [46]:

$$\varphi_{\nu_\alpha}(E) = \frac{\beta^\beta}{\Gamma(\beta)} \frac{E^{\beta-1}}{\langle E_{\nu_\alpha} \rangle^\beta} e^{-\beta E / \langle E_{\nu_\alpha} \rangle}, \quad (3)$$

where β is a spectral parameter, and $\Gamma(\beta)$ is the Euler gamma function. The values of the parameters are model dependent (e.g. see the Fig. 3 in [32]). For our numerical illustrations, we choose

$$(\langle E_{\nu_e} \rangle, \langle E_{\bar{\nu}_e} \rangle, \langle E_{\nu_x} \rangle) = (12, 15, 18) \text{ MeV}, \quad (4)$$

and $\beta = 4$, from the admissible parameter ranges [46].

We will consider three representative cases for the ratios of the neutrino fluxes, namely

$$\begin{aligned} \Phi_{\nu_e}^0 : \Phi_{\bar{\nu}_e}^0 : \Phi_{\nu_x}^0 &= 2.40 : 1.60 : 1.0, \\ \Phi_{\nu_e}^0 : \Phi_{\bar{\nu}_e}^0 : \Phi_{\nu_x}^0 &= 0.85 : 0.75 : 1.0, \\ \Phi_{\nu_e}^0 : \Phi_{\bar{\nu}_e}^0 : \Phi_{\nu_x}^0 &= 0.81 : 0.79 : 1.0. \end{aligned} \quad (5)$$

The first case represents a flux ordering with a ν_e dominance, typical of the accretion phase, practically producing a single-crossed spectrum. The other two cases

¹ We mention that recently multi-angle effects have been included also in the study of the flavor evolution of the ν_e neutronization burst in O-Ne-Mg supernovae. We address the interested reader to [41].

represent fluxes possible during the cooling phase, with a moderate ν_x dominance and different flavor asymmetries, producing a multiple-crossed spectrum. We will see how multi-angle effects would have a different impact for these three cases.

B. Equations of motion

Mixed neutrinos are described by matrices of density $\rho_{\mathbf{p}}$ and $\bar{\rho}_{\mathbf{p}}$ for each (anti)neutrino mode. The diagonal entries are the usual occupation numbers whereas the off-diagonal terms encode phase information. We are studying the spatial evolution of the neutrino fluxes in a quasi-stationary situation. Therefore, the matrices $\rho_{\mathbf{p}}$ do not explicitly depend on time, so that the evolution reduces to the Liouville term involving only spatial derivatives. Moreover, we assume spherical symmetry so that the only relevant spatial variable is the radial coordinate r . In this case, the explicit form of the equations of motion (EoMs) has been obtained in [4, 5, 19, 36, 47, 48].

$$i\mathbf{v}_{\mathbf{p}} \cdot \nabla_r \rho_{\mathbf{p}} = [\mathbf{H}_{\mathbf{p}}, \rho_{\mathbf{p}}] , \quad (6)$$

where $\mathbf{v}_{\mathbf{p}}$ is the velocity and the Hamiltonian reads

$$\mathbf{H}_{\mathbf{p}} = \Omega_{\mathbf{p}} + \mathbf{V}_{\text{MSW}} + \mathbf{V}_{\nu\nu} . \quad (7)$$

In a three flavor scenario, the matrix of the vacuum oscillation frequencies for neutrinos is $\Omega_{\mathbf{p}} = \text{diag}(m_1^2, m_2^2, m_3^2)/2|\mathbf{p}|$ in the mass basis. For antineutrinos $\Omega_{\mathbf{p}} \rightarrow -\Omega_{\mathbf{p}}$. It will prove convenient to cast the matrix of vacuum oscillation frequencies in its traceless form

$$\Omega_{\omega} = -\frac{\omega}{\sqrt{3}} \lambda_8 - \alpha \frac{\omega}{2} \lambda_3 \quad (8)$$

where λ_3 and λ_8 are the two diagonal Gell-Mann matrices, which read respectively [45]

$$\begin{aligned} \lambda_3 &= \text{diag}(1, -1, 0) , \\ \lambda_8 &= \frac{1}{\sqrt{3}} \text{diag}(1, 1, -2) . \end{aligned}$$

The vacuum oscillation frequency

$$\omega = \frac{\Delta m_{\text{atm}}^2}{2E} \quad (9)$$

is associated to the atmospheric mass-square difference $\Delta m_{\text{atm}}^2 = m_3^2 - m_{1,2}^2$. The mass hierarchy parameter is

$$\alpha \equiv \text{sgn}(\Delta m_{\text{atm}}^2) \frac{\Delta m_{\text{sol}}^2}{\Delta m_{\text{atm}}^2} , \quad (10)$$

$\Delta m_{\text{sol}}^2 = m_2^2 - m_1^2$ being the solar mass-square difference. $\Delta m_{\text{atm}}^2 > 0$ defines the normal mass hierarchy (NH), while $\Delta m_{\text{atm}}^2 < 0$ the inverted hierarchy (IH). For

the numerical illustrations, we take the neutrino mass-squared differences to be $|\Delta m_{\text{atm}}^2| = 2 \times 10^{-3} \text{ eV}^2$ and $\Delta m_{\text{sol}}^2 = 8 \times 10^{-5} \text{ eV}^2$, close to their current best-fit values [49]. In SN neutrino flavor conversions, the parameters $(\Delta m_{\text{atm}}^2, \theta_{13})$ are responsible of conversions between $e - y$ states, while $(\Delta m_{\text{sol}}^2, \theta_{12})$ determine conversions between $e - x$ states [45]. The mass hierarchy implies the dominance of $e - y$ conversion effects over the $e - x$ ones. However, are possible situations in which one finds an interesting interplay between the “atmospheric” and “solar” sectors [30, 31], as we will show in the following.

The matter effect in Eq. (7), due to the background electron density n_e , in the weak interaction basis $(\nu_e, \nu_{\mu}, \nu_{\tau})$ is represented by [1]

$$\mathbf{V}_{\text{MSW}} = \sqrt{2} G_F n_e \text{diag}(1, 0, 0) . \quad (11)$$

Except at very early times ($t \lesssim 300 \text{ ms}$) when the effective electron density n_e would become larger than the neutrino density n_{ν} suppressing the self-induced flavor conversions [50], one can account for matter effects in the region of collective oscillations just by choosing small (matter suppressed) mixing angles [17, 50], which we take to be $\theta_{13} = \theta_{12} = 10^{-3}$. Matter effects in the region of collective oscillations (up to a few 100 km) also slightly modify the neutrino mass-square differences. Therefore, we take the effective mass-square differences $\Delta \tilde{m}_{\text{atm}}^2 = \Delta m_{\text{atm}}^2 \cos \theta_{13} \simeq \Delta m_{\text{atm}}^2$ and $\Delta \tilde{m}_{\text{sol}}^2 = \Delta m_{\text{sol}}^2 \cos \theta_{12} \simeq 0.4 \Delta m_{\text{sol}}^2$ [26, 50]. Mikheyev-Smirnov-Wolfenstein (MSW) conversions typically occur after collective effects have ceased [21, 45]. Their effects then factorize and can be included separately [2]. Therefore, we neglect them in the following.

Finally, the effective potential due to the neutrino-neutrino interactions is given by [3–5, 34]

$$\mathbf{V}_{\nu\nu} = \sqrt{2} G_F \int \frac{d^3 \mathbf{q}}{(2\pi)^3} (\rho_{\mathbf{q}} - \bar{\rho}_{\mathbf{q}}) (1 - \mathbf{v}_{\mathbf{p}} \cdot \mathbf{v}_{\mathbf{q}}) , \quad (12)$$

where the factor $(1 - \mathbf{v}_{\mathbf{p}} \cdot \mathbf{v}_{\mathbf{q}})$ implies *multi-angle* effects for neutrinos moving on different trajectories [18], as explained in Sec. I.

We will solve the EoM’s in the multi-angle case and compare the behavior of the flavor evolution with the solution obtained in the *single-angle* approximation [18]. This latter requires the occurrence of the self-maintained coherence of the neutrino ensemble, i.e. that at a given location all the neutrino modes are aligned with each other, assuming they were aligned at the source [47]. In this case one obtains an angle-averaged EoM for the different energy modes, classified in terms of the frequency ω

$$i\partial_r \rho_{\omega} = [\mathbf{H}_{\omega}, \rho_{\omega}] , \quad (13)$$

where we have defined the “reduced neutrino density matrix” as [26]

$$\rho_{\omega} \sim \begin{cases} +\rho_{\mathbf{q}} & \text{if } \omega > 0 \\ -\bar{\rho}_{\mathbf{q}} & \text{if } \omega < 0 \end{cases} , \quad (14)$$

whose diagonal components

$$\rho_{\omega(\alpha\alpha)}(r) = \frac{F_{\nu\alpha}(\omega, r)}{F_{\nu}(\omega, r)} , \quad (15)$$

are normalized to the sum of the fluxes of all the neutrino species $F_{\nu}(\omega, r) = F_{\nu_e}(E, r) + F_{\nu_x}(E, r) + F_{\nu_y}(\omega, r)$ (and analogously for antineutrinos). We clarify that when we use the ω -variable, with the notation $F_{\nu}(\omega)$ we would mean $F_{\nu}(E) \times dE/d\omega$.

Neglecting the matter effects, the single-angle Hamiltonian reads [47]

$$H_{\omega} = \Omega_{\omega_r} + \mu_r^* \rho . \quad (16)$$

In this equation the vacuum oscillation frequency ω when projected over the radial direction becomes [47]

$$\omega_r = \frac{\omega}{\langle v_r \rangle} , \quad (17)$$

where

$$\langle v_r \rangle = \frac{1}{2} \left[1 + \sqrt{1 - \left(\frac{R}{r} \right)^2} \right] \quad (18)$$

is the angle-averaged radial neutrino velocity. The modification of the vacuum oscillation frequencies is relevant only near the neutrinosphere, therefore in the following we neglect it in our estimations.

The neutrino-neutrino interaction term depends on the matrix of total density

$$\rho = \frac{1}{\Phi_{\nu}^0 + \Phi_{\bar{\nu}}^0} \int_{-\infty}^{+\infty} d\omega F_{\nu} \rho_{\omega} \quad (19)$$

normalized to the sum of the total neutrinos and antineutrinos flux at the neutrinosphere.

The radial dependence of the neutrino-neutrino interaction strength can be written as [21, 47]

$$\mu_r^* = \mu_R \frac{R^2}{2r^2} C_r , \quad (20)$$

where

$$\mu_R = 2\pi\sqrt{2}G_F(\Phi_{\nu}^0 + \Phi_{\bar{\nu}}^0) , \quad (21)$$

represents the strength of the neutrino-neutrino potential at the neutrinosphere. The r^{-2} scaling comes from the geometrical flux dilution, and the collinearity factor

$$\begin{aligned} C_r &= 4 \left[\frac{1 - \sqrt{1 - (R/r)^2}}{(R/r)^2} \right]^2 - 1 \\ &\approx \frac{1}{2} \left(\frac{R}{r} \right)^2 \quad \text{for } r \rightarrow \infty , \end{aligned} \quad (22)$$

arises from the $(1 - \cos\theta)$ structure of the neutrino-neutrino interaction. The asymptotic behavior for large

r agrees with what one obtains by considering that all neutrinos are launched at 45° to the radial-direction [36]. The known decline of the neutrino-neutrino interaction strength, $\mu_r^* \sim r^{-4}$ for $r \gg R$, is evident [3].

The behavior of the neutrino ensemble at large densities in the single-angle case can be characterized in terms of the invariants of the system. Namely, two *lepton-numbers*, which for small in-medium mixing angles read in flavor basis [26, 51]

$$\begin{aligned} \mathcal{L}_3 &= \frac{1}{\Phi_{\nu}^0 + \Phi_{\bar{\nu}}^0} \int_{-\infty}^{+\infty} d\omega F_{\nu} \text{Tr}(\rho_{\omega} \lambda_3) \\ \mathcal{L}_8 &= \frac{1}{\Phi_{\nu}^0 + \Phi_{\bar{\nu}}^0} \int_{-\infty}^{+\infty} d\omega F_{\nu} \text{Tr}(\rho_{\omega} \lambda_8) , \end{aligned} \quad (23)$$

and the *effective energy* of the system [35]

$$\mathcal{E} = -\frac{1}{\sqrt{3}} \text{Tr}(\tilde{\rho} \lambda_8) - \frac{\alpha}{2} \text{Tr}(\tilde{\rho} \lambda_3) + \frac{\mu_r^*}{2} \text{Tr}(\rho^2) , \quad (24)$$

where

$$\tilde{\rho} = \frac{1}{\Phi_{\nu}^0 + \Phi_{\bar{\nu}}^0} \int_{-\infty}^{+\infty} d\omega \omega F_{\nu} \rho_{\omega} , \quad (25)$$

is the first momentum of the density matrix.

III. MULTI-ANGLE EFFECTS FOR DIFFERENT NEUTRINO FLUXES

In this Section we compare the results of the SN neutrino flavor evolution, obtained using the single-angle [Eq. (13)] and multi-angle [Eq. (6)] EoM's for the three representative SN flux models introduced in Eq. (5). For the sake of brevity, we will show only results of the supernova neutrino flavor evolution in the case of inverted neutrino mass hierarchy. We think that this case is more interesting, since possible three-flavor effects, associated with Δm_{sol}^2 have been recently found in the single-angle scheme for SN neutrino fluxes with multiple crossing points [30, 31]. We will show that multi-angle effects can strongly suppress the impact of these three-flavor conversions.

In our numerical simulations we fix the value of the neutrino-neutrino interaction strength at the neutrinosphere

$$\mu_r^*(R) = 2.1 \times 10^6 \text{ km}^{-1} , \quad (26)$$

unless otherwise stated. This choice will imply that neutrino luminosities in the three different cases will be (in units of 10^{51} erg/s)

$$\begin{aligned} L_{\nu_e} &= 2.40 , \quad L_{\bar{\nu}_e} = 2.00 , \quad L_{\nu_x} = 1.50 , \\ L_{\nu_e} &= 1.20 , \quad L_{\bar{\nu}_e} = 1.34 , \quad L_{\nu_x} = 2.14 , \\ L_{\nu_e} &= 1.16 , \quad L_{\bar{\nu}_e} = 1.41 , \quad L_{\nu_x} = 2.14 . \end{aligned} \quad (27)$$

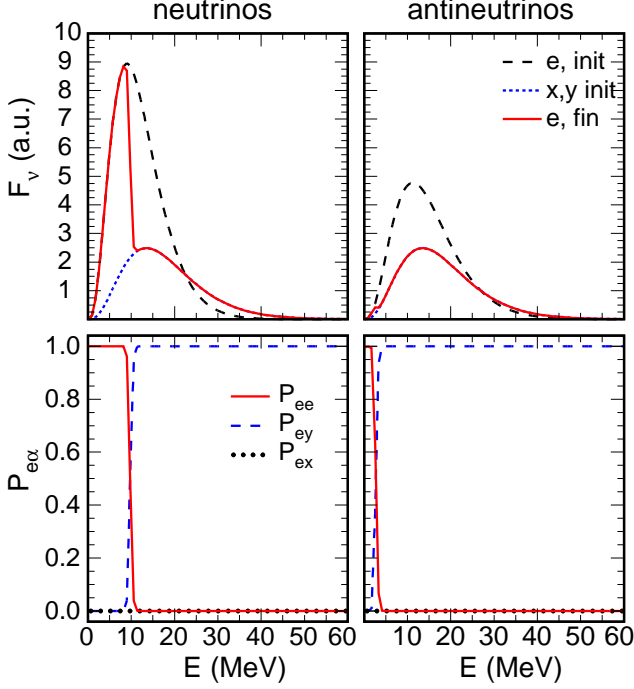


FIG. 1: Case with $\Phi_{\nu_e}^0 : \Phi_{\bar{\nu}_e}^0 : \Phi_{\nu_x}^0 = 2.40 : 1.60 : 1.0$. Three-flavor evolution in inverted mass hierarchy for the *single-angle* case for neutrinos (left panels) and antineutrinos (right panels). Upper panels: Initial energy spectra for ν_e (long-dashed curve) and $\nu_{x,y}$ (short-dashed curve) and for ν_e after collective oscillations (solid curve). Lower panels: probabilities P_{ee} (solid red curve), P_{ey} (dashed blue curve), P_{ex} (dotted black curve).

In order to get stable results in our multi-angle simulations we typically use ~ 1500 angular modes. Finally, to saturate self-induced oscillation effects, we integrate the EoM's till $r = 10^3$ km. Technical details are discussed in the Appendix: in the following we focus only on the results and their interpretation.

A. Spectrum with a single crossing

We start our investigation with the SN neutrino flux ordering $\Phi_{\nu_e}^0 : \Phi_{\bar{\nu}_e}^0 : \Phi_{\nu_x}^0 = 2.40 : 1.60 : 1.0$, as representative of the accretion phase. This case has been the benchmark for most of the previous multi-angle studies (see, e.g., [18, 21]). As known, in this case the dynamics can be studied into the $e - y$ two-neutrino system associated with $(\Delta m_{\text{atm}}^2, \theta_{13})$. Three-flavor effects in the $e - x$ sector, associated with $(\Delta m_{\text{sol}}^2, \theta_{12})$ are negligible [45, 52].

In Fig. 1 we represent the initial neutrino fluxes at the neutrinosphere for all the different species and the final electron (anti)neutrino fluxes after collective oscillations (at $r = 10^3$ km) in the single-angle approximation (upper

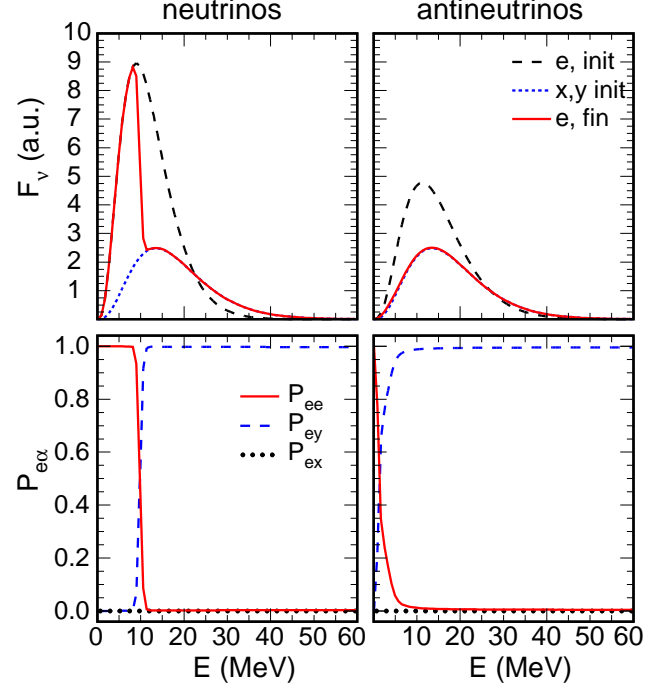


FIG. 2: As in Fig. 1, but for the *multi-angle* case.

panels) and the corresponding $P_{ee} = P(\nu_e \rightarrow \nu_e)$, $P_{ex} = P(\nu_e \rightarrow \nu_x)$ and $P_{ey} = P(\nu_e \rightarrow \nu_y)$ conversion probabilities (lower panels). Neutrinos are shown in the left panels and antineutrinos in the right panels. The corresponding results for the multi-angle case are given in Fig. 2. We stress that, except in the high-energy tails, the original neutrino spectra in the case under study always have an excess of electron (anti)neutrinos over the non-electron species, i.e. $F_{\nu_e} > F_{\nu_x}$ and $F_{\bar{\nu}_e} > F_{\bar{\nu}_x}$. In the frequency variable $-\infty < \omega < +\infty$, the crossing point at $E \rightarrow \infty$ ($\omega = 0$) and the other two at $E \gtrsim 20$ MeV appear so narrowly spaced, that the neutrino spectra superficially appear with only a *single crossing* point at $\omega = 0$, where $F_{\nu_e} = F_{\nu_x} = 0$ and $F_{\bar{\nu}_e} = F_{\bar{\nu}_x} = 0$. We address the interested reader to Fig. 3 of [29] and to the relative discussion on the case neutrino spectrum effectly behaving as a single-crossing one. We will show how this property is crucial in characterizing the flavor evolution.

Concerning the neutrino fluxes after self-induced oscillations, in the single-angle case one finds a swap between ν_e and ν_y spectra above $E \simeq 10$ MeV, producing the typical split in the final neutrino spectra. For antineutrinos, the swap between $\bar{\nu}_e$ and $\bar{\nu}_y$ is almost complete, the splitting energy $E \simeq 2$ MeV being very low. Neglecting this low-energy feature [22], the position of the ν_e split can be calculated using the conservation of the lepton number \mathcal{L}_8 in Eq. (23) (see, e.g., [23–25]). In the multi-angle case, the swap features remain unchanged, except for the smearing of the low-energy anti-neutrino spectral split, shown also in [22].

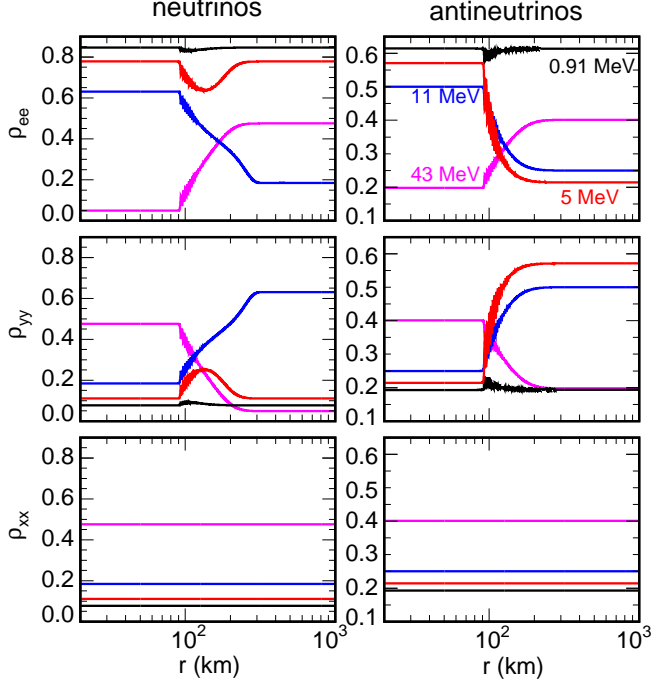


FIG. 3: Case with $\Phi_{\nu_e}^0 : \Phi_{\nu_e}^0 : \Phi_{\nu_x}^0 = 2.40 : 1.60 : 1.0$. Three-flavor evolution in inverted mass hierarchy in the *single-angle* case. Radial evolution of the diagonal components of the density matrix ρ for neutrinos (left panels) and antineutrinos (right panels) for different energy modes.

In Fig. 3 and 4 we represent the radial evolution of the diagonal elements of the density matrix ρ_{ee} , ρ_{yy} , ρ_{xx} for different energy modes for neutrinos (left panels) and antineutrinos (right panels). In particular, in the ρ_{ee} panels the order of the energy modes is $E = 0.91, 5, 11, 43$ MeV going from the curve starting with the highest value to the lowest one. This order is reversed in the ρ_{yy} and ρ_{xx} panels. Figure 3 represents the single-angle evolution, while Fig. 4 is for the multi-angle evolution, where the density matrix elements have been integrated over the angular distribution. Except for very low-energy antineutrino modes, we find that the evolution of the density matrix is rather similar in the single-angle and multi-angle case. We find the presence of synchronized oscillations [8, 19] till $r \simeq 85$ km. Till there all the ρ_ω stay pinned to their original value.

Significant flavor conversions start only after synchronization when bipolar oscillations [19] start to swap the flavor content of the system. The synchronization radius can be found through the condition [21]

$$\mu_r^* > \frac{4}{\sqrt{3}} \frac{\omega_s \text{Tr}(\sigma\lambda_8)}{[\text{Tr}(\rho\lambda_8)]^2}. \quad (28)$$

Using the alignment approximation for the two blocks of neutrinos and antineutrinos, the synchronization

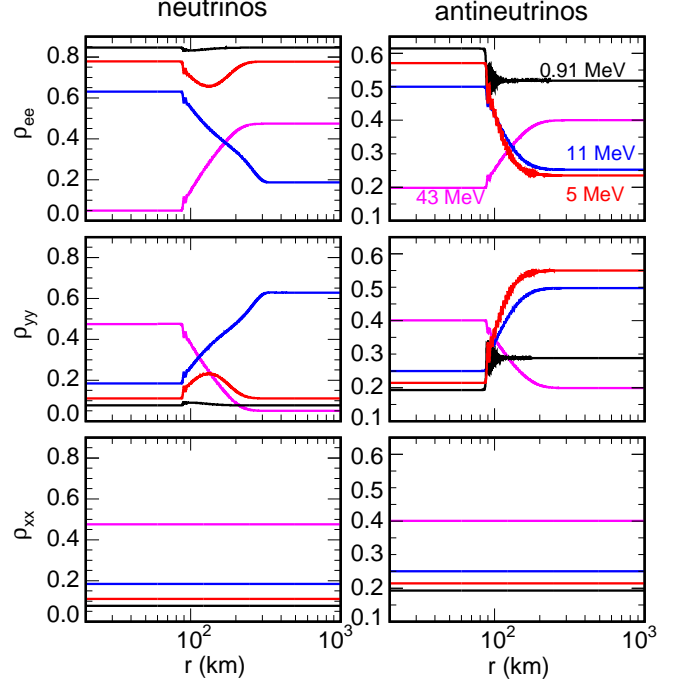


FIG. 4: As in Fig. 3, but for the *multi-angle* case.

frequency for $e - y$ conversions, reads [21]

$$\begin{aligned} \omega_s &= \frac{\int_0^{+\infty} d\omega \, \omega (F_{\nu_e}^0(E) - F_{\nu_y}^0(\omega))}{2(\Phi_{\nu_e}^0 - \Phi_{\nu_y}^0)} \\ &+ \frac{\int_0^{+\infty} d\omega \, \omega (F_{\bar{\nu}_e}^0(\omega) - F_{\bar{\nu}_y}^0(\omega))}{2(\Phi_{\bar{\nu}_e}^0 - \Phi_{\bar{\nu}_y}^0)} \\ &= \frac{2\Delta m_{\text{atm}}^2}{3} \left[\frac{L_{\nu_e}/\langle E_{\nu_e} \rangle^2 - L_{\nu_x}/\langle E_{\nu_x} \rangle^2}{L_{\nu_e}/\langle E_{\nu_e} \rangle - L_{\nu_x}/\langle E_{\nu_x} \rangle} \right. \\ &\quad \left. + \frac{L_{\bar{\nu}_e}/\langle E_{\bar{\nu}_e} \rangle^2 - L_{\nu_x}/\langle E_{\nu_x} \rangle^2}{L_{\bar{\nu}_e}/\langle E_{\bar{\nu}_e} \rangle - L_{\nu_x}/\langle E_{\nu_x} \rangle} \right] \\ &\simeq 0.68 \text{ km}^{-1}, \end{aligned}$$

for our input fluxes. The function

$$\sigma = \frac{1}{\Phi_{\nu}^0 + \Phi_{\bar{\nu}}^0} \int_{-\infty}^{+\infty} d\omega \, \text{sgn}(\omega) F_{\nu} \rho_{\omega}.$$

Then

$$\begin{aligned} \text{Tr}(\sigma\lambda_8) &= \frac{\rho_{ee} + \bar{\rho}_{ee} - 2\rho_{xx}}{\sqrt{3}} = \\ &= \frac{1}{\sqrt{3}} \frac{L_{\nu_e}\langle E_{\bar{\nu}_e} \rangle\langle E_{\nu_x} \rangle + L_{\bar{\nu}_e}\langle E_{\nu_e} \rangle\langle E_{\nu_x} \rangle - 2L_{\nu_x}\langle E_{\bar{\nu}_e} \rangle\langle E_{\nu_e} \rangle}{L_{\nu_e}\langle E_{\nu_x} \rangle\langle E_{\bar{\nu}_e} \rangle + L_{\bar{\nu}_e}\langle E_{\nu_e} \rangle\langle E_{\nu_x} \rangle + 4L_{\nu_x}\langle E_{\nu_e} \rangle\langle E_{\bar{\nu}_e} \rangle} \\ &\simeq 0.144, \end{aligned}$$

and

$$\text{Tr}(\rho\lambda_8) = \frac{\rho_{ee} - \bar{\rho}_{ee}}{\sqrt{3}} =$$

$$\begin{aligned}
&= \frac{1}{\sqrt{3}} \frac{\langle E_{\nu_x} \rangle [L_{\nu_e} \langle E_{\bar{\nu}_e} \rangle - L_{\bar{\nu}_e} \langle E_{\nu_e} \rangle]}{L_{\nu_e} \langle E_{\nu_x} \rangle \langle E_{\bar{\nu}_e} \rangle + L_{\bar{\nu}_e} \langle E_{\nu_e} \rangle \langle E_{\nu_x} \rangle + 4L_{\nu_x} \langle E_{\nu_e} \rangle \langle E_{\bar{\nu}_e} \rangle} \\
&\simeq 0.06.
\end{aligned}$$

These numbers imply that bipolar conversions would start when $\mu_r^* \simeq 100 \omega_H$, i.e. at $r \simeq 85$ km, as observed in the Fig. 3.

We stress that the presence of synchronization at low-radii in this case is crucially related with the original spectrum with a single crossing point. As discussed in [43], energy conservation at large neutrino densities (i.e. when $\mu_r^* \rightarrow \infty$) implies that ρ^2 and thus ρ are conserved [see Eq. (24)], and therefore behave as collective objects. If ρ is conserved, energy conservation implies that also $\text{Tr}(\tilde{\rho}\lambda_8)$ has to be conserved (neglecting the subleading three-flavor effects associated to Δm_{sol}^2). For a single-crossed spectrum, the quantity $\text{Tr}(\tilde{\rho}\lambda_8) = [(\tilde{\rho}_{ee} - \tilde{\rho}_{yy}) + (\tilde{\rho}_{ee} - \tilde{\rho}_{yy})]/\sqrt{3}$ is maximal [29]. Therefore moving any energy mode ρ_ω from its initial value would make the energy of the system larger. In this situation, each ρ_ω must remain pinned with the global density matrix ρ . Therefore, only the synchronization among different modes is possible [43]. Since during the synchronization phase the different ρ_ω remain aligned to their original value, multi-angle effects are suppressed.

Then, during the phase of the spectral swapping, the spectrum near the crossing point acts like an inverted pendulum [29]. The swap sweeps through the spectrum on each side of the crossing, and the modes at the edge of the swap precess at an average oscillation frequency $\kappa \simeq \Delta m_{\text{atm}}^2/2E \simeq 0.5 \text{ km}^{-1}$ for a typical energy $E \simeq 10 \text{ MeV}$ in the region of the swap. Since, the length scale $l_\mu \equiv |d \ln \mu_r^*(r)/dr|^{-1} = r/4$ is larger than κ^{-1} , the evolution is adiabatic concerning the swapping dynamics [30, 31]. However, the time-scale of multi-angle effects is determined by the bipolar oscillation frequency $\omega_H \sim \sqrt{2\omega\mu_r^*} \sim r^{-2}$ [35] that decreases faster than l_μ^{-1} . Qualitatively, the effect of the synchronization is to postpone conversions at large radii, where multi-angle effects would require more “time” to develop since μ_r^* is smaller, and the relatively fast decrease of μ_r^* would reduce the adiabaticity for multi-angle effects. As a consequence these do not grow significantly. This is qualitatively the origin of the so called “quasi single-angle” behavior [36], observed for neutrino flux ordering typical of the accretion phase. We have explicitly checked that modifying artificially the adiabaticity of the evolution, i.e. choosing a very slow decrease of μ_r^* multi-angle decoherence is unavoidable also in the case we are considering. Therefore, as suggested in [36], the absence of multi-angle decoherence during the accretion phase seems due to a luckily conspiracy of different time-scales. Unfortunately, till now it has not been developed yet a complete theory for that. Therefore, the interpretation of these effects is mostly based on the experience gained through numerical observations.

B. Spectrum with multiple crossings

We pass now to the case $\Phi_{\nu_e}^0 : \Phi_{\bar{\nu}_e}^0 : \Phi_{\nu_x}^0 = 0.85 : 0.75 : 1.0$ representative of recent simulation results for the neutrino flux ordering during the cooling phase [38]. This case has been widely studied in the single-angle approximation in [29–31] and corresponds to spectra that in ω variable present well separated multiple crossings, in which multiple spectral splits can arise around the crossing points (see Fig. 2 of [29]). Moreover, in this case peculiar three-flavor effects, associated with conversions between e and x states have been recently discussed [30, 31]. Multi-angle simulations in this case have shown a smearing of the splitting features [29, 42] and a suppression the flavor evolution at low-radii [42, 44].

In Fig. 5 we show the initial (anti)neutrino spectra for all the flavors and the final electron (anti)neutrino ones for the single-angle case (upper panels) and the corresponding conversion probabilities at the end of the flavor evolution. Multi-angle results are shown in Fig. 6. Starting with the single-angle case, we see that both $\nu_e \leftrightarrow \nu_y$ as well as $\bar{\nu}_e \leftrightarrow \bar{\nu}_y$ swaps appear at intermediate energies $5 \text{ MeV} \lesssim E \lesssim 20 \text{ MeV}$. Moreover, for $E \gtrsim 25 \text{ MeV}$, there are additional $\nu_e \leftrightarrow \nu_x$ and $\bar{\nu}_e \leftrightarrow \bar{\nu}_x$ swaps. As result of this complex dynamics, in the single-angle case the oscillated ν_e spectrum shows a single split, the one at low-energies, producing the swap with ν_y after the split, while the high-energy split is canceled by the further swap between ν_e and ν_x . We observe that in the antineutrino sector the spectral swaps are not complete, due to smaller spectral differences between $\bar{\nu}_e$ and $\bar{\nu}_x$ that lead to a less adiabatic evolution, as explained in [31].

Passing to the multi-angle case, the differences with the single-angle case in the final neutrino spectra and in the conversion probabilities are significant. In general, all the splitting features are less pronounced than in the single-angle case. Starting with the neutrino case, we see that the low-energy spectral split is smeared. More remarkably, the high-energy swap between ν_e and ν_x is strongly suppressed. As a consequence, the final neutrino spectra keep track only of the swap between ν_e and ν_y , which now is less sharp than in the single-angle case. This effect would produce a high-energy splitting feature in the final ν_e spectrum at $E \simeq 25 \text{ MeV}$, not present in the single-angle three-flavor calculations. For antineutrinos, the impact of multi-angle effects is even stronger: flavor transformations are significantly suppressed, except in the energy range close to crossing point of the spectra, where two-flavor $\bar{\nu}_e \rightarrow \bar{\nu}_y$ transformations take place.

To explain the above observations, we represent the radial evolution of the diagonal elements of the density matrix ρ_{ee} , ρ_{yy} , ρ_{xx} for different energy modes, for neutrinos (left panels) and antineutrinos (right panels) in Figs. 7 and 8. Figure 7 represents the single-angle case, while Fig. 8 represents the multi-angle case. In this latter case, the density matrix elements have been integrated over the angular distribution. In the ρ_{ee} panels the order of the energy modes is $E = 3.3, 5.7, 19, 30 \text{ MeV}$ going

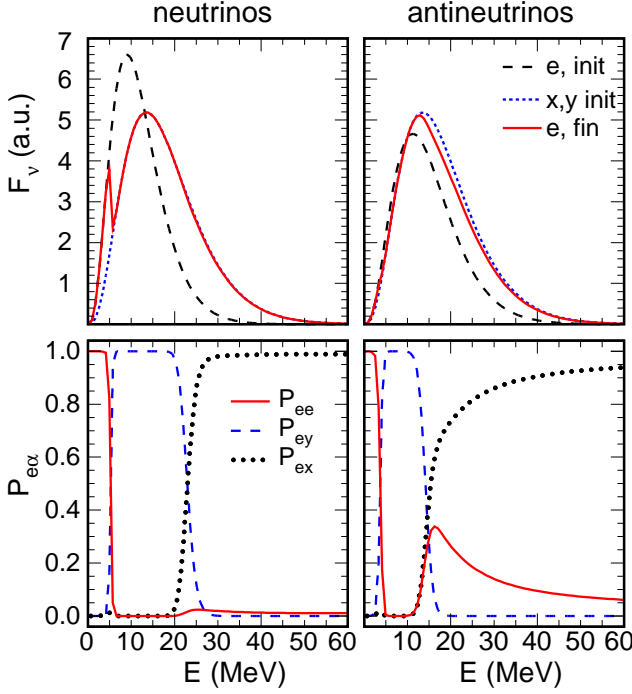


FIG. 5: Case with $\Phi_{\nu_e}^0 : \Phi_{\nu_e}^0 : \Phi_{\nu_x}^0 = 0.85 : 0.75 : 1.0$. Three-flavor evolution in the *single-angle* case for neutrinos (left panels) and antineutrinos (right panels). Upper panels: Initial energy spectra for ν_e (long-dashed curve) and $\nu_{x,y}$ (short-dashed curve) and for ν_e after collective oscillations (solid curve). Lower panels: probabilities P_{ee} (solid red curve), P_{ey} (dashed blue curve), P_{ex} (dotted black curve).

from the curve starting with the highest value to the lowest one. This order is reversed in the ρ_{yy} and ρ_{xx} panels. Starting with the single-angle case, we see that differently from the case studied in the Sec. III A, flavor conversions are possible at low radii ($r \gtrsim 30$ km) in a region where we would have expected synchronization. The effect of the small in-medium mixing is only to logarithmically delay the onset of the flavor conversions.

As explained in [43], the crucial difference with respect to the previous case is that, applying the energy conservation [Eq. (24)] to the case of multiple-crossed spectra, it is possible to conserve $\text{Tr}(\bar{\rho}\lambda_8)$ and $\alpha\text{Tr}(\bar{\rho}\lambda_3)$, by flipping parts of the original neutrino spectra around the crossing points. Therefore, the synchronization behavior found in the case of single-crossed spectra is not necessarily stable in this case. Indeed, in [43] it has been discussed the possibility of a novel form of flavor conversions for large μ_r^* in terms of a self-induced *parametric resonance* that would destabilize the synchronization. The origin of this effect is that since each ρ_ω would precess around the Hamiltonian H_ω with a frequency μ_r^* , H_ω itself must vibrate with the same frequency. In this situation, for large μ_r^* the total density matrix ρ continues to behave as a collective object, but

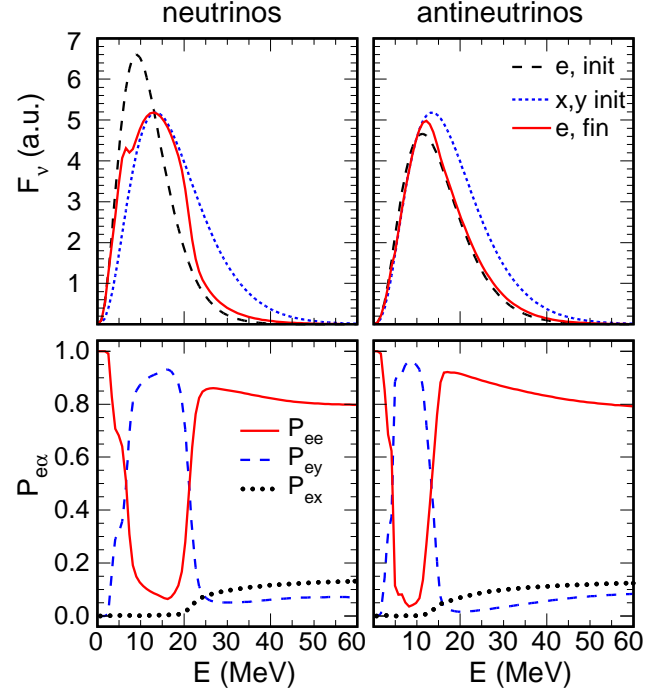


FIG. 6: As in Fig. 5, but for the *multi-angle* case.

is not static and vibrates itself with a frequency μ_r^* . For single-crossed spectra, the energy conservation prevents any sizable change in the different ρ_ω , therefore the synchronized behavior prevails. Conversely, in presence of multiple-crossed neutrino spectra, the different ρ_ω 's do not remain aligned with the global ρ and start to librate relative to each other.

We also note that in this case three-flavor effects, associated with $(\Delta m_{\text{sol}}^2, \theta_{12})$ are present. In particular, from the figure, one realizes that collective librations first start in the $e-y$ system (at $r \gtrsim 30$ km), and then trigger the $e-x$ conversions (at $r \gtrsim 60$ km). The explanation of this dynamics has been recently given in [31], where we redirect the interested reader.

Passing to the multi-angle case of Fig. 8, we find that now the low-radii flavor conversions are suppressed. This effect has been recently described in [42], even if there it has not made the connection between this behavior and the multi-angle suppression of the parametric resonance. This effect has been pointed out in [43] for generic neutrino gases with half-isotropic neutrino distributions, in cases where in the single-angle scheme the parametric resonance was found. The point is that in the multi-angle case, for large μ_r^* the different ρ_ω 's would precess with different velocities whose spread, due to multi-angle effects, is much larger than ω . As a consequence of this dispersion, there cannot exist a collective parametric resonance for all the neutrino modes. Therefore, the collective behavior found in the idealized single-angle case is “fragile” and easily suppressed by multi-angle

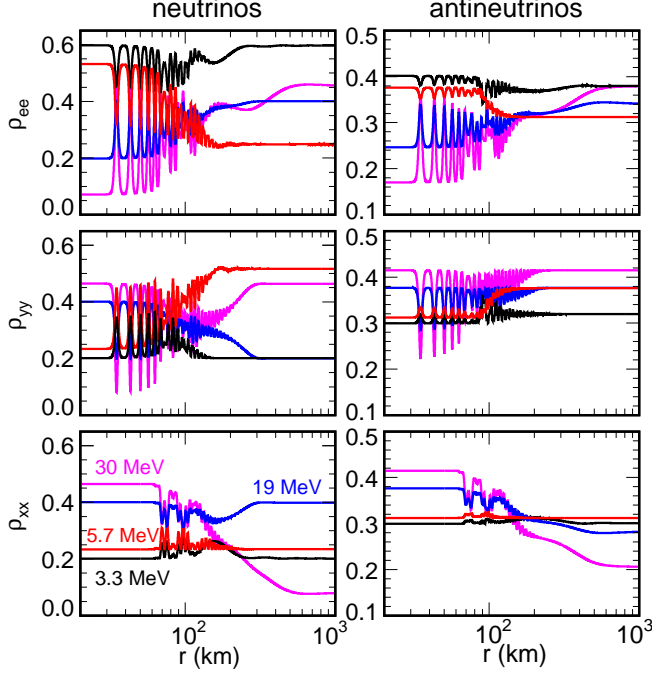


FIG. 7: Case with $\Phi_{\nu_e}^0 : \Phi_{\bar{\nu}_e}^0 : \Phi_{\nu_x}^0 = 0.85 : 0.75 : 1.0$. Three-flavor evolution in inverted mass hierarchy in single-angle case. Radial evolution of the diagonal components of the density matrix ρ for neutrinos (left panels) and antineutrinos (right panels) for different energy modes.

effects in the realistic anisotropic supernova environment. In this case, as long as multi-angle effects are dominant, they would suppress any flavor conversion at small radii. As discussed in [42], the role of multi-angle effects in this case is analogous to the one that they have in presence of a large matter term ($n_e \gg n_\nu$) [50]. There, multi-angle effects introduce a significant dispersion for the matter potential encountered by neutrinos on different trajectories, that once more would suppress self-induced conversions.

In the presence of multi-angle suppression, we expect that flavor conversions would start only when neutrino-neutrino interactions are not strong enough to maintain the collective behavior of ρ [42]. Neutrino modes would remain frozen to their initial condition, till the neutrino-neutrino interaction μ_r^* becomes comparable with the averaged vacuum oscillation frequency of the neutrino ensemble [45]

$$\langle \omega \rangle = \frac{\text{Tr}(\tilde{\rho}\lambda_8)}{\text{Tr}(\rho\lambda_8)} = \frac{\tilde{\rho}_{ee} + \tilde{\bar{\rho}}_{ee} - 2\tilde{\rho}_{yy}}{\rho_{ee} - \bar{\rho}_{ee}}, \quad (29)$$

where for our input spectra

$$= \frac{\tilde{\rho}_{ee} + \tilde{\bar{\rho}}_{ee} - 2\tilde{\rho}_{yy}}{3} \frac{L_{\nu_e}/\langle E_{\nu_e} \rangle^2 + L_{\bar{\nu}_e}\langle E_{\bar{\nu}_e} \rangle^2 - 2L_{\nu_x}/\langle E_{\nu_x} \rangle^2}{L_{\nu_e}/\langle E_{\nu_e} \rangle + L_{\bar{\nu}_e}\langle E_{\bar{\nu}_e} \rangle + 4L_{\nu_x}/\langle E_{\nu_x} \rangle}$$

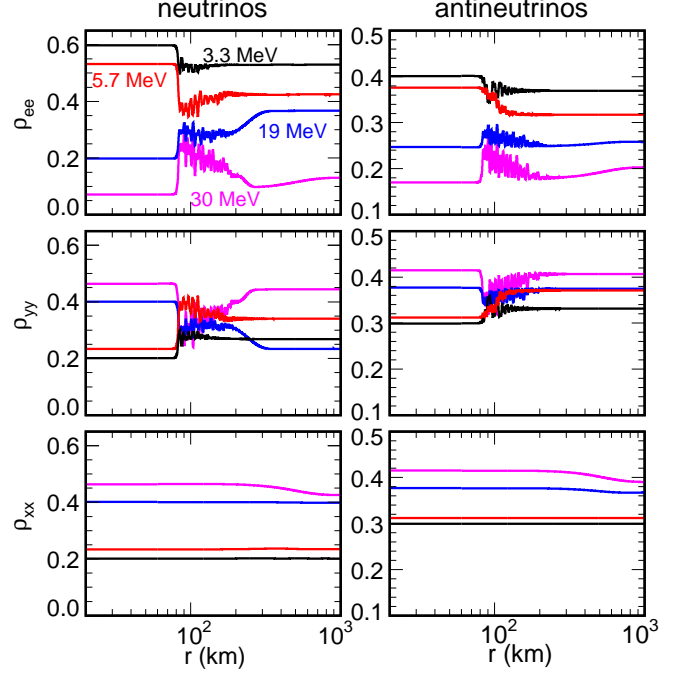


FIG. 8: As in Fig. 7, but for the *multi-angle* case.

$$\simeq 1.1 \times 10^{-2} \text{ km}^{-1},$$

and

$$\begin{aligned} & \rho_{ee} - \bar{\rho}_{ee} \\ &= \frac{L_{\nu_e}\langle E_{\bar{\nu}_e} \rangle\langle E_{\nu_x} \rangle + L_{\bar{\nu}_e}\langle E_{\nu_e} \rangle\langle E_{\nu_x} \rangle - 2L_{\nu_x}\langle E_{\bar{\nu}_e} \rangle\langle E_{\nu_e} \rangle}{L_{\nu_e}\langle E_{\nu_x} \rangle\langle E_{\bar{\nu}_e} \rangle + L_{\bar{\nu}_e}\langle E_{\nu_e} \rangle\langle E_{\nu_x} \rangle + 4L_{\nu_x}\langle E_{\nu_e} \rangle\langle E_{\bar{\nu}_e} \rangle} \\ &\simeq 1.6 \times 10^{-2}, \end{aligned} \quad (30)$$

which numerically leads to $\langle \omega \rangle \simeq 0.68 \text{ km}^{-1}$.

We expect flavor conversions to start in the $e-y$ sector when

$$\langle \omega \rangle \simeq \sqrt{3}\mu_r^* \text{Tr}(\rho\lambda_8), \quad (31)$$

that would correspond to $\mu_r^* \simeq 60 \langle \omega \rangle$. For our input spectra, we would get as onset radius $r_{\text{ons}} \simeq 92 \text{ km}$, in qualitative agreement with the simulation of Fig. 8. We note that numerically the conversions' onset radius in this case is very similar to the one of Sec. III A, even if the conditions that determine it are different, as well as the further flavor evolution. In particular, we expect that at large radii the evolution in this case would be less adiabatic than in the case of Sec. III A. As explained in [29], in the final phases of the swapping dynamics, the neutrino and antineutrino spectra evolve quite independently, and the precession frequencies of the two blocks are not governed by a common μ_r^* , but by individual μ_r^* 's proportional to

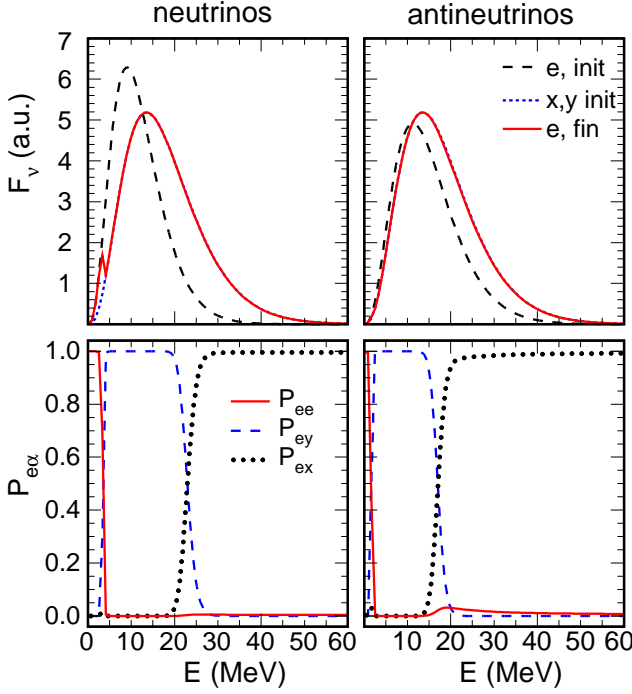


FIG. 9: Case with $\Phi_{\nu_e}^0 : \Phi_{\nu_e}^0 : \Phi_{\nu_x}^0 = 0.81 : 0.79 : 1.0$. Three-flavor evolution in the *single-angle* case for neutrinos (left panels) and antineutrinos (right panels). Upper panels: Initial energy spectra for ν_e (long-dashed curve) and $\nu_{x,y}$ (short-dashed curve) and for ν_e after collective oscillations (solid curve). Lower panels: probabilities P_{ee} (solid red curve), P_{ey} (dashed blue curve), P_{ex} (dotted black curve).

the flux differences $|F_{\nu_e} - F_{\nu_x}|$ ($|F_{\bar{\nu}_e} - F_{\bar{\nu}_x}|$). They behave essentially as two uncoupled oscillators because the neutrino-neutrino interaction μ_r^* is now smaller than the frequency difference of the two blocks. Since in this case the flux differences are smaller than in the previous example of Sec. III A, the effective precession frequencies are smaller, with a resultant less adiabatic evolution. This would explain the more pronounced smearing of the sharp splitting features observed in this case in the multi-angle simulations.

The effect of the multi-angle delay is that flavor conversions start in a region in which the neutrino-neutrino interaction strength is weaker than in the corresponding single-angle case. The typical time-scale at which the off-diagonal components in the density matrix grow is given by the bipolar period which, for $e - y$ transitions, is $\tau_H \sim (2\omega\mu_r^*)^{-1/2}$ [19]. The delay of the conversions means that they start at a smaller μ_r^* where they require more time to develop. Moreover, going at larger r makes the evolution less adiabatic, resulting in weaker flavor conversions than in the single-angle case. This would explain the suppression of the $e - x$ conversions. At this regard, we remind that $e - x$ conversions are triggered by the dominant $e -$

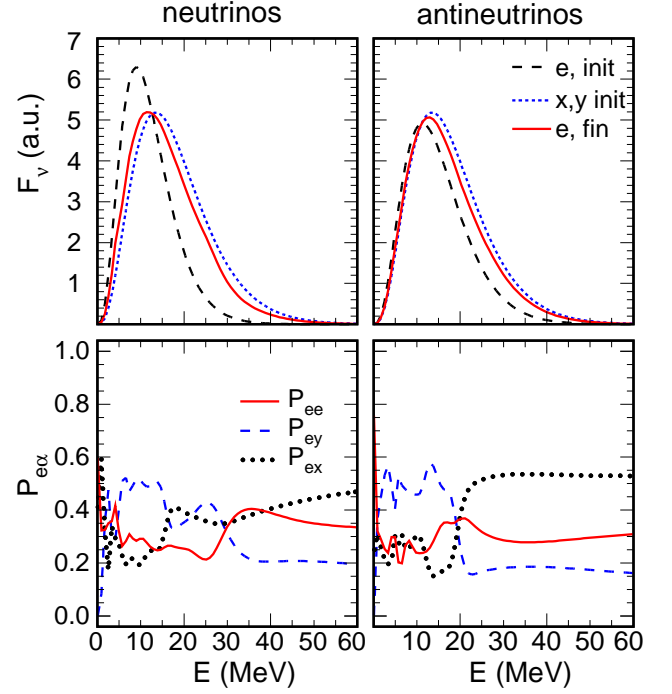


FIG. 10: As in Fig. 9, but for the *multi-angle* case.

y conversions, via the θ_{13} coupling between the two sectors [31]. Due to the suppression of $e - y$ conversions, the $e - x$ transitions would also be delayed. The typical time-period at which the off-diagonal components in the $e - x$ sector grow, is $\tau_L \sim (\alpha\omega\mu_r^*)^{-1/2}$. The mass hierarchy implies that $\tau_L \simeq 8\tau_H$. As a consequence of this slower growth of the $e - x$ conversions, the multi-angle suppression is enough to make τ_L too slow to be effective.

The suppression of conversions between ν_e and ν_x explains the appearance of the high-energy spectral split in ν_e observed in the multi-angle case of Fig. 7. Concerning antineutrinos, we realize that not only $e - x$, but also $e - y$ conversions are strongly inhibited. We associate this behavior with the stronger violation of adiabaticity in the antineutrino sector, due to the smaller spectral differences among $\bar{\nu}_e$ and $\bar{\nu}_x$ [31].

We stress that the adiabaticity plays a crucial role in determining the impact of the multi-angle suppression in the flavor evolution. Indeed, we explicitly checked that for the same flux ordering, increasing the adiabaticity, by increasing the neutrino-neutrino potential by a factor of five, the multi-angle suppression is less dramatic. In particular, $e - x$ conversions reappear. Moreover, also the suppression of flavor oscillations in the antineutrino sector is relieved. We find that this result is in agreement with the case shown in [42]. There the choice of higher neutrino luminosities with respect to the ones we are considering as benchmark case, allows the multi-angle suppression to be strong only at low-radii, while the final

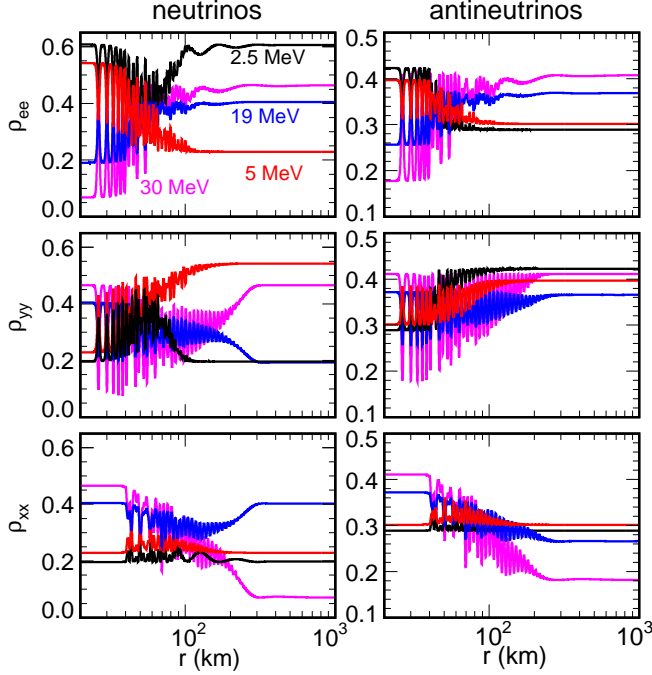


FIG. 11: Case with $\Phi_{\nu_e}^0 : \Phi_{\bar{\nu}_e}^0 : \Phi_{\nu_x}^0 = 0.81 : 0.79 : 1.0$. Three-flavor evolution in inverted mass hierarchy in single-angle case. Radial evolution of the diagonal components of the density matrix ρ for neutrinos (left panels) and antineutrinos (right panels) for different energy modes.

spectra are similar to the ones obtained in the single-angle case.

C. Spectrum with small flavor asymmetries

Finally, we consider the case $\Phi_{\nu_e}^0 : \Phi_{\bar{\nu}_e}^0 : \Phi_{\nu_x}^0 = 0.81 : 0.79 : 1.0$ which is intended to represent a case which a flux ordering possible at late times, where asymmetries among ν_e and $\bar{\nu}_e$ can become small [39, 40]. The small asymmetry case has been pointed as representative of flavor decoherence associated to multi-angle effects [35, 36].

In Fig. 9 show the initial (anti)neutrino spectra for all the flavors and the final electron (anti)neutrino ones for the single-angle case (upper panels) and the corresponding conversion probabilities at the end of the flavor evolution. Multi-angle results are shown in Fig. 10. The splitting features in the single-angle case are similar to the ones observed in Fig. 5 of Sec. III B. However, the multi-angle results are dramatically different. We observe that neutrino and antineutrino spectra tend toward flavor equilibration with different conversion probabilities displaced around 1/3.

In Fig. 11 and 12 we represent the radial evolution of the diagonal elements of the density matrix ρ_{ee} , ρ_{yy} ,

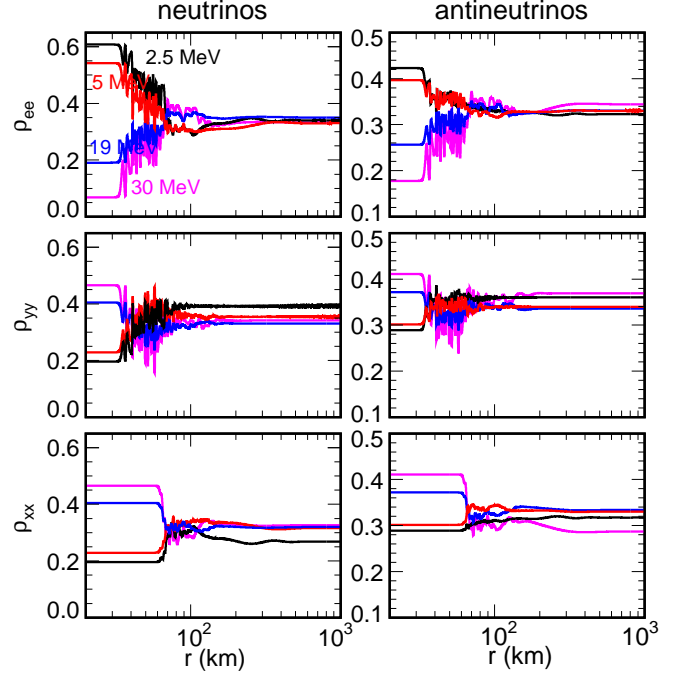


FIG. 12: As in Fig. 11, but for the *multi-angle* case.

ρ_{xx} for different energy modes for neutrinos (left panels) and antineutrinos (right panels). In the ρ_{ee} panels the order of the energy modes is $E = 2.5, 5, 19, 30$ MeV going from the curve starting with the highest value to the lowest one. This order is reversed in the ρ_{yy} and ρ_{xx} panels. Figure 11 represents the single-angle case, while Fig. 12 represents the multi-angle case. The difference of the flavor evolution in the two cases is striking. In particular, multi-angle suppression blocks e - y flavor conversions till $r \simeq 40$ km, as predictable from Eq. (31). Then, since conversions start at small r where the evolution is more adiabatic than in the case of Sec. III B, also e - x oscillations have chance to develop at $r \gtrsim 60$ km. The stronger adiabaticity in this case allow also multi-angle effects to have enough time to develop before the neutrino-neutrino interaction term becomes small. Then, the multi-angle effects smear the flavor conversions, producing a tendency towards a three-flavor decoherence of the ensemble in both ν and $\bar{\nu}$ sectors.

IV. CONCLUSIONS

We have performed an exploration on the dependence of multi-angle effects in self-induced supernova neutrino oscillations on the original neutrino fluxes. Most of the previous studies [18, 21, 22, 36] focused on neutrino fluxes typical of the accretion phase, with a pronounced ν_e excess, *de facto* behaving like spectra with a single crossing. In this situation, the synchronization of

TABLE I: Summary of multi-angle effects, 3ν effects and spectral splts for different SN neutrino fluxes.

Initial spectral pattern	Multi-angle effects	Δm_{sol}^2 -effects	Spectral splts
Single crossing	marginal	absent	robust
Multiple crossings	relevant	present/absent	smeared
Small flavor asymmetries	strong	present	washed-out

different angular modes at low-radii prevails over multi-angle effects. Then, when flavor conversions start, these are adiabatic to produce the spectral swaps and splits, but not enough to allow multi-angle decoherence to emerge. The result is the known “quasi single-angle” evolution.

However, one has to be cautious in generalizing this reassuring result. In this context, we have shown that multi-angle effects can produce significant deviations in the flavor evolution with respect to the three-flavor single-angle case, for neutrino fluxes with a moderate flavor hierarchy and a ν_x excess, as possible during the supernova cooling phase. In this situation, the presence of multiple crossing points in the original neutrino spectra destabilizes the synchronization at large neutrino densities [43]. In absence of synchronization, in the single-angle scheme collective conversions would be possible at low-radii. However, multi-angle effects introduce a large dispersion in the neutrino-neutrino potential, that prevents any possible collective flavor conversion at low radii. As a consequence, in the multi-angle scheme there would be a significant delay of the onset of the flavor conversions, as recently observed [42]. We have shown that this multi-angle delay can produce dramatic changes, not only in the deepest supernova regions, as shown in [42], but also in the final oscillated neutrino spectra. In particular, the multi-angle suppression can be so strong to allow the onset of the flavor evolution only at a large radius, when the evolution is less adiabatic. Depending on the violation of adiabaticity, in the inverted mass hierarchy there could be a suppression of the three-flavor effects, associated to the solar sector. This would dramatically change the pattern of swaps and splits in the final neutrino spectra. Finally, if the flavor asymmetries between ν_e and $\bar{\nu}_e$ are very small, the multi-angle suppression occurs only close to the neutrinosphere. In this situation, the stronger adiabaticity of the evolution allows multi-angle effects to act efficiently also after the onset of the conversions, tending to establish a three-flavor equilibration in both neutrino and antineutrino sectors.

In Table I we summarize our results on the role of multi-angle effects, 3ν effects and spectral splits for different SN neutrino fluxes. In this work we have explicitly shown numerical results only for the case of neutrino inverted mass hierarchy. However, we have checked that the impact of multi-angle effects is qualitatively similar also for the normal hierarchy case.

From our numerical explorations, it results that self-induced flavor transformations of supernova neutrinos during the cooling phase are a continuous source of surprises. The richness of the phenomenology, in the presence of neutrino spectra with multiple crossing points, was first realized in [29] with the discovery of the possibility of multiple spectral splits in both the mass hierarchies. Then, it was realized that for these neutrino fluxes, three-flavor effects can play a significant role in inverted mass hierarchy, changing the splitting pattern expected from two-flavor calculations [30, 31]. Now, we show that also multi-angle effects are crucial in characterizing the flavor evolution in this case, and could potentially kill the three-flavor effects. In general, self-induced flavor conversions for spectra with multiple crossing points challenge most of the naive expectations on which was based the original picture of the collective supernova neutrino conversions: low-radii synchronization, subleading role of multi-angle and three-flavor effects.

The discovery of these new effects adds additional layers of complications in the simulation of the flavor evolution for supernova neutrinos. In particular, our result shows that during the cooling phase three-flavor multi-angle simulations are crucial to obtain a correct result. Multi-angle effects would be taken into account to assess the impact of collective neutrino oscillations on the r-process nucleosynthesis in supernovae, as recently investigated in [53]. The impact of the multi-angle effects would crucially depend on different SN input: neutrino luminosities and flavor asymmetries, neutrinosphere radius, etc. Since all these quantities significantly change during the neutrino emission, one would expect time-dependent effects. At this regard, the possibility to detect signatures of these effects in the next galactic supernova neutrino burst [33] would motivate further analytical and numerical investigations.

Appendix

We discuss here a few technical aspects of the multi-angle numerical simulations, we performed on our local computer facility (with Fortran 77 codes running a Linux cluster with 48 processors per CPU with 128 Gb of shared RAM memory). Equation (6), after discretization, provides a set of $16 \times N_E \times N_u$ ordinary differential equations in r , where N_E and N_u are the

number of points sampling the (anti)neutrino energy E and emission angle. In particular, we find convenient to label the neutrino angular modes in terms of the variable [36]

$$u = \sin^2 \theta_R, \quad (32)$$

where θ_R is the zenith angle at the neutrino sphere $r = R$ of a given mode relative to the radial direction. With this choice, the parameter u is fixed for every neutrino trajectory.

We have then performed our simulations of the three-flavor neutrino evolution using a Runge-Kutta integration routine taken from the CERNLIB libraries [54]. We fixed the numerical tolerance of the integrator at the level of 10^{-6} and increased the number of sampling points in angle and energy till we reach a stable numerical result. In this situation we estimate a numerical (fractional) accuracy of our results better than 10^{-2} . In order to have a clear energy resolution of the spectral splits we took $N_E = 10^2$ energy points, equally distributed in the range $E \in [0.1, 80]$ MeV. The number of angular modes is

also a crucial choice, since it is well known that a sparse sampling in angle can lead to numerical artifacts that would destroy the collective behavior of the neutrino self-induced conversions [36]. Typically, numerical stability would require $N_u = \mathcal{O}(10^3)$ angular modes.

Since we can claim to have reached stable numerical simulations, we are confident in the accuracy of the results obtained in this work. Moreover, we have been able to reproduce previous results presented in literature for cases similar to the ones we are investigating (see, e.g., [21, 42]).

Acknowledgments

We thank Sovan Chakraborty, Basudeb Dasgupta and Georg Raffelt for reading the manuscript and for comments on it. The work of A.M. was supported by the German Science Foundation (DFG) within the Collaborative Research Center 676 “Particles, Strings and the Early Universe”.

-
- [1] L. Wolfenstein, “Neutrino Oscillations In Matter,” *Phys. Rev. D* **17**, 2369 (1978); S. P. Mikheev and A. Yu. Smirnov, “Resonance Enhancement Of Oscillations In Matter And Solar Neutrino Spectroscopy,” *Yad. Fiz.* **42**, 1441 (1985) [*Sov. J. Nucl. Phys.* **42**, 913 (1985)].
 - [2] A. S. Dighe and A. Y. Smirnov, “Identifying the neutrino mass spectrum from the neutrino burst from a supernova,” *Phys. Rev. D* **62**, 033007 (2000) [hep-ph/9907423].
 - [3] J. Pantaleone, “Neutrino oscillations at high densities,” *Phys. Lett. B* **287**, 128 (1992).
 - [4] G. Sigl and G. Raffelt, “General kinetic description of relativistic mixed neutrinos,” *Nucl. Phys. B* **406**, 423 (1993).
 - [5] B. H. J. McKellar and M. J. Thomson, “Oscillating doublet neutrinos in the early universe,” *Phys. Rev. D* **49**, 2710 (1994).
 - [6] Y. Z. Qian and G. M. Fuller, “Neutrino-neutrino scattering and matter enhanced neutrino flavor transformation in Supernovae,” *Phys. Rev. D* **51**, 1479 (1995) [astro-ph/9406073].
 - [7] S. Samuel, “Neutrino oscillations in dense neutrino gases,” *Phys. Rev. D* **48**, 1462 (1993).
 - [8] V. A. Kostelecký and S. Samuel, “Neutrino oscillations in the early universe with an inverted neutrino mass hierarchy,” *Phys. Lett. B* **318**, 127 (1993).
 - [9] V. A. Kostelecký and S. Samuel, “Self-maintained coherent oscillations in dense neutrino gases,” *Phys. Rev. D* **52**, 621 (1995) [hep-ph/9506262].
 - [10] S. Samuel, “Bimodal coherence in dense selfinteracting neutrino gases,” *Phys. Rev. D* **53**, 5382 (1996) [hep-ph/9604341].
 - [11] S. Pastor, G. G. Raffelt and D. V. Semikoz, “Physics of synchronized neutrino oscillations caused by self-interactions,” *Phys. Rev. D* **65**, 053011 (2002) [hep-ph/0109035].
 - [12] Y. Y. Y. Wong, “Analytical treatment of neutrino asymmetry equilibration from flavour oscillations in the early universe,” *Phys. Rev. D* **66**, 025015 (2002) [hep-ph/0203180].
 - [13] K. N. Abazajian, J. F. Beacom and N. F. Bell, “Stringent constraints on cosmological neutrino antineutrino asymmetries from synchronized flavor transformation,” *Phys. Rev. D* **66**, 013008 (2002) [arXiv:astro-ph/0203442].
 - [14] S. Pastor and G. Raffelt, “Flavor oscillations in the supernova hot bubble region: Nonlinear effects of neutrino background,” *Phys. Rev. Lett.* **89**, 191101 (2002) [astro-ph/0207281].
 - [15] R. F. Sawyer, “Classical instabilities and quantum speed-up in the evolution of neutrino clouds,” hep-ph/0408265.
 - [16] R. F. Sawyer, “Speed-up of neutrino transformations in a supernova environment,” *Phys. Rev. D* **72**, 045003 (2005) [hep-ph/0503013].
 - [17] H. Duan, G. M. Fuller and Y. Z. Qian, “Collective Neutrino Flavor Transformation In Supernovae,” *Phys. Rev. D* **74**, 123004 (2006) [astro-ph/0511275].
 - [18] H. Duan, G. M. Fuller, J. Carlson and Y. Z. Qian, “Simulation of coherent non-linear neutrino flavor transformation in the supernova environment. I: Correlated neutrino trajectories,” *Phys. Rev. D* **74**, 105014 (2006) [astro-ph/0606616].
 - [19] S. Hannestad, G. G. Raffelt, G. Sigl and Y. Y. Y. Wong, “Self-induced conversion in dense neutrino gases: Pendulum in flavour space,” *Phys. Rev. D* **74**, 105010 (2006) [Erratum-ibid. *D* **76**, 029901 (2007)] [astro-ph/0608695].
 - [20] H. Duan, G. M. Fuller and Y. Z. Qian, “Collective Neutrino Oscillations,” arXiv:1001.2799 [hep-ph].
 - [21] G. L. Fogli, E. Lisi, A. Marrone and A. Mirizzi, “Collective neutrino flavor transitions in supernovae and the role of trajectory averaging,” *JCAP* **0712**, 010 (2007) [arXiv:0707.1998 [hep-ph]].
 - [22] G. L. Fogli, E. Lisi, A. Marrone, A. Mirizzi and I. Tamborra, “Low-energy spectral features of supernova

- (anti)neutrinos in inverted hierarchy,” *Phys. Rev. D* **78**, 097301 (2008) [arXiv:0808.0807 [hep-ph]].
- [23] G. G. Raffelt and A. Y. Smirnov, “Self-induced spectral splits in supernova neutrino fluxes,” *Phys. Rev. D* **76**, 081301 (2007) [Erratum-ibid. *D* **77**, 029903 (2008)] [arXiv:0705.1830 [hep-ph]].
- [24] G. G. Raffelt, A. Y. Smirnov, “Adiabaticity and spectral splits in collective neutrino transformations,” *Phys. Rev. D* **76**, 125008 (2007). [arXiv:0709.4641 [hep-ph]].
- [25] H. Duan, G. M. Fuller, J. Carlson *et al.*, “Neutrino Mass Hierarchy and Stepwise Spectral Swapping of Supernova Neutrino Flavors,” *Phys. Rev. Lett.* **99**, 241802 (2007). [arXiv:0707.0290 [astro-ph]].
- [26] H. Duan, G. M. Fuller, Y. -Z. Qian, “Stepwise spectral swapping with three neutrino flavors,” *Phys. Rev. D* **77**, 085016 (2008). [arXiv:0801.1363 [hep-ph]].
- [27] J. Gava and C. Volpe, “Collective neutrinos oscillation in matter and CP-violation,” *Phys. Rev. D* **78**, 083007 (2008) [arXiv:0807.3418 [astro-ph]].
- [28] J. Gava, J. Kneller, C. Volpe and G. C. McLaughlin, “A dynamical collective calculation of supernova neutrino signals,” *Phys. Rev. Lett.* **103**, 071101 (2009) [arXiv:0902.0317 [hep-ph]].
- [29] B. Dasgupta, A. Dighe, G. G. Raffelt and A. Y. Smirnov, “Multiple Spectral Splits of Supernova Neutrinos,” *Phys. Rev. Lett.* **103**, 051105 (2009) [arXiv:0904.3542 [hep-ph]].
- [30] A. Friedland, “Self-refraction of supernova neutrinos: mixed spectra and three-flavor instabilities,” *Phys. Rev. Lett.* **104**, 191102 (2010) [arXiv:1001.0996 [hep-ph]].
- [31] B. Dasgupta, A. Mirizzi, I. Tamborra and R. Tomàs, “Neutrino mass hierarchy and three-flavor spectral splits of supernova neutrinos,” *Phys. Rev. D* **81**, 093008 (2010) [arXiv:1002.2943 [hep-ph]].
- [32] G. Fogli, E. Lisi, A. Marrone and I. Tamborra, “Supernova neutrinos and antineutrinos: ternary luminosity diagram and spectral split patterns,” *JCAP* **0910**, 002 (2009) [arXiv:0907.5115 [hep-ph]].
- [33] S. Choubey, B. Dasgupta, A. Dighe and A. Mirizzi, “Signatures of collective and matter effects on supernova neutrinos at large detectors,” arXiv:1008.0308 [hep-ph].
- [34] J. T. Pantaleone, “Dirac neutrinos in dense matter,” *Phys. Rev. D* **46**, 510 (1992).
- [35] G. G. Raffelt and G. Sigl, “Self-induced decoherence in dense neutrino gases,” *Phys. Rev. D* **75**, 083002 (2007) [hep-ph/0701182].
- [36] A. Esteban-Pretel, S. Pastor, R. Tomàs, G. G. Raffelt and G. Sigl, “Decoherence in supernova neutrino transformations suppressed by deleptonization,” *Phys. Rev. D* **76**, 125018 (2007) [arXiv:0706.2498 [astro-ph]].
- [37] R. F. Sawyer, “The multi-angle instability in dense neutrino systems,” *Phys. Rev. D* **79** (2009) 105003 [arXiv:0803.4319 [astro-ph]].
- [38] G. G. Raffelt, M. T. Keil, R. Buras, H. T. Janka and M. Rampp, “Supernova neutrinos: Flavor-dependent fluxes and spectra,” astro-ph/0303226.
- [39] T. Fischer, S. C. Whitehouse, A. Mezzacappa *et al.*, “Protoneutron star evolution and the neutrino driven wind in general relativistic neutrino radiation hydrodynamics simulations,” *Astron. Astrophys.* **517**, A80 (2010). [arXiv:0908.1871 [astro-ph.HE]].
- [40] L. Hudepohl, B. Muller, H. -T. Janka *et al.*, “Neutrino Signal of Electron-Capture Supernovae from Core Collapse to Cooling,” *Phys. Rev. Lett.* **104**, 251101 (2010). [arXiv:0912.0260 [astro-ph.SR]].
- [41] J. F. Cherry, G. M. Fuller, J. Carlson, H. Duan and Y. Z. Qian, “Multi-Angle Simulation of Flavor Evolution in the Neutrino Neutronization Burst From an O-Ne-Mg Core-Collapse Supernova,” *Phys. Rev. D* **82** (2010) 085025 [arXiv:1006.2175 [astro-ph.HE]].
- [42] H. Duan and A. Friedland, “Self-induced suppression of collective neutrino oscillations in a supernova,” *Phys. Rev. Lett.* **106**, 091101 (2011) [arXiv:1006.2359 [hep-ph]].
- [43] G. G. Raffelt, “Self-induced parametric resonance in collective neutrino oscillations,” *Phys. Rev. D* **78** (2008) 125015 [arXiv:0810.1407 [hep-ph]].
- [44] Animated figures at <http://www.mppmu.mpg.de/supernova/multisplits/>
- [45] B. Dasgupta and A. Dighe, “Collective three-flavor oscillations of supernova neutrinos,” *Phys. Rev. D* **77**, 113002 (2008) [arXiv:0712.3798 [hep-ph]].
- [46] M. T. Keil, G. G. Raffelt and H. T. Janka, “Monte Carlo study of supernova neutrino spectra formation,” *Astrophys. J.* **590**, 971 (2003) [astro-ph/0208035].
- [47] B. Dasgupta, A. Dighe, A. Mirizzi and G. G. Raffelt, “Collective neutrino oscillations in non-spherical geometry,” *Phys. Rev. D* **78**, 033014 (2008) [arXiv:0805.3300 [hep-ph]].
- [48] H. Duan, G. M. Fuller, Y. -Z. Qian, “Symmetries in collective neutrino oscillations,” *J. Phys. G* **G36**, 105003 (2009). [arXiv:0808.2046 [astro-ph]].
- [49] M. C. Gonzalez-Garcia, M. Maltoni and J. Salvado, “Updated global fit to three neutrino mixing: status of the hints of $\theta_{13} > 0$,” *JHEP* **1004** (2010) 056 [arXiv:1001.4524 [hep-ph]].
- [50] A. Esteban-Pretel, A. Mirizzi, S. Pastor, R. Tomàs, G. G. Raffelt, P. D. Serpico and G. Sigl, “Role of dense matter in collective supernova neutrino transformations,” *Phys. Rev. D* **78**, 085012 (2008) [arXiv:0807.0659 [astro-ph]].
- [51] B. Dasgupta, A. Dighe, A. Mirizzi and G. G. Raffelt, “Spectral split in prompt supernova neutrino burst: Analytic three-flavor treatment,” *Phys. Rev. D* **77**, 113007 (2008). [arXiv:0801.1660 [hep-ph]].
- [52] G. Fogli, E. Lisi, A. Marrone and I. Tamborra, “Supernova neutrino three-flavor evolution with dominant collective effects,” *JCAP* **0904**, 030 (2009). [arXiv:0812.3031 [hep-ph]].
- [53] H. Duan, A. Friedland, G. C. McLaughlin and R. Surman, “The influence of collective neutrino oscillations on a supernova r-process,” arXiv:1012.0532 [astro-ph.SR].
- [54] <http://dollywood.itp.tuwien.ac.at/cernlib/>